Effects of Pulsation on the Flow Field of Turbulent Impinging Jets

H. Medina*

Coventry University, Coventry, CV1 5FB, United Kingdom

E. Benard†

Department of Aerospace Engineering, University of Glasgow, Glasgow, G12 8QQ, United Kingdom

J.M. Early‡

The Queen's University of Belfast, Belfast, BT9 5AH, United Kingdom

The current study examines the effect of pulsation on the flow field of turbulent impinging jets. Previous work identified significant differences in the transitional and turbulent jet responses to pulsation, and this study considers the effect of the Strouhal number on the structure of turbulent impinging jets. This is of particular interest due to the widespread use of jets (for instance, in heat and mass transfer applications), and there is an interest in the utilisation of pulsating jets as alternative to steady jets to increase heat and mass transfer rates. Preliminary findings suggest that in order to achieve improvements in heat and mass transfer rates, a turbulent jet is preferable to an equivalent transitional jet as their behaviour is easier to predict, and for a number of frequencies, they exhibit favourable flow conditions when compared to the equivalent steady jet case. The similariry in the observed turbulence characteristics between the steady and pulsating cases also suggests that a steady jet model could be a viable baseline for computational modelling of a turbulent pulsating jet.

Nomenclature

A_N	Pulse amplitude, U_{rms}/U_{avg}
d	Nozzle diameter, m
H	Nozzle-to-plate spacing, m
Re	Reynolds number
r	Radial distance from stagnation point, m
St	Strouhal number
T_{avg}	Average temperature $(T_1 + T_2)/2$, °C
T_r	Room temperature, °C
T_1	Experiment start temperature, °C
T_2	Experiment start temperature, °C
U_e	Time-averaged centreline exit velocity, m/s
u, v	Instantaneous axial and radial velocity components, m/s
u', v'	Mean axial and radial turbulent velocity components, m/s
x	Axial distance from nozzle exit, m

Subscripts

max	Cycle maximum velocity
min	Cycle minimum velocity

*Senior Lecturer, School of Mechanical and Automotive Engineering

†Senior Lecturer, Department of Aerospace Engineering, University of Glasgow

‡Lecturer, The Queen's University of Belfast, AIAA Senior Member

rms Root mean square
Abbreviations
PIV Particle image velocimetry
TKE Turbulent kinetic energy

I. Introduction

When the development of a free-jet flow (generated when a fluid is discharged from a nozzle into an ambient fluid) is interrupted by the prescence of a surface, an impinging jet is created. Impinging jets are characterised by a rapid deceleration of the discharged fluid as it reaches the surface. This deceleration leads to high rates of momentum, heat and mass transfer, consequently, impinging jets have found a place in many industrial applications (for example, cooling of electronics, inner surfaces of turbine blades, etc).

Due to the numerous practical applications of impinging jets, their study has been mainly oriented towards understanding their mass, momentum and heat transfer characteristics.[1,2] However, an understanding of the underlying fluid mechanics behind these types of jet also offers significant benefits to the study of free shear layers and boundary layers. Furthermore, from a modelling perspective, the study of impinging jets can be incorporated into the development of turbulence models, as most are tested on flows which are parallel to the wall (and as such are not equipped to deal with flows in which the streamlines are orientated close to orthogonal). Even though efforts to improve computational models have been made, they are being held back by the lack of detailed experimental data[3] as a large quantity of the research on impinging jets is still mainly oriented towards understanding the heat transfer characteristics of impinging jets at high Reynolds numbers since they lead to the highest rates of heat transfer.

The study of these jet structures has been further complicated by the numerous configurations which are encountered, which has often led to contradictions in the obsrevations made about their behaviour.[4] Of more interest is the possibility that the use of a pulsating, rather than steady, impinging jet can enhance the heat transfer rates, but again, this has not been conclusively proven and evidence does exist to contradict this, demonstrating the pulsation has a detrimental effect on the heat transfer characteristics.,[5,6].[7] While these discrepancies in the heat transfer characteristics exist, there is in addition a fundamental lack of research on the velocity and turbulent fields of these jet structures. There are only a few works available that study the velocity field of pulsed, but the focus is still firmly on the heat transfer mechanims, with limited velocity data presented. jets.[8,9] It is therefore evident that due to the large number of potential experimental configurations, and the contradictions observed throughout the literature for both steady and pulsating jets, there is a need for both a systematic approach to the study of impinging jets and an in-depth study of the flow field and fluid mechanics. This will not only serve as a basis to understanding how the velocity field might affect heat transfer, but also to provide data for turbulence model validation. The current paper presents the results of an experimental study conducted into the effects of pulsation on the flow field of a turbulent impinging jet, examining the effects of varying the non-dimensional frequency of the pulsation.

II. Experimental Setup and Procedure

A. Experimental Facility

The experiments were undertaken in a custom built water facility at the Queen's University of Belfast. This facility operates on a recirculating principle in which it relies on a gravity-fed mechanism to generate the jet. An overhead tank provides the required head, and the water passes through the pulsator (the valve remains fully opened for the steady jet experiments) and the nozzle inlet, before finally exiting at the test section into the main water tank. The excess water from the main tank is collected into a reservoir tank and is pumped back up to the overhead tank in order to maintain a constant water level in the head tank (necessary to keep a steady supply of water to the test section). A schematic of the experimental apparatus can be seen in figure 1.

The test section is constructed as a rectangular glass tank (inner dimensions $605.6mm$ long, $302.8mm$ tall and $300.8mm$ wide), with a wall thickness of $2mm$ (capable of holding approximately 55 litres of water). Glass was a convenient material because it allows visual access to the test section.

In order to ensure a fully developed exit profile, a round nozzle (d_inner=$30.5mm$) of 50 diameters in

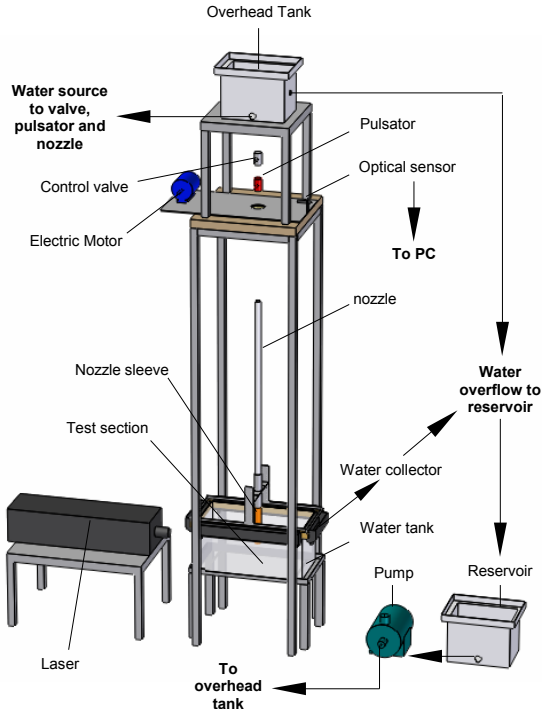

Figure 1. Experimental Facility Overview

length was utilised. The first 40 diameters(1,220mm) consist of a straight PVC tube (to prevent rusting and ensure no degradation of the inner wall quality). However, for the last 10 diameters (305mm) of the nozzle a sleeve was used to ensure that the inner section of the nozzle remained circular.

A custom-built pulsator was used to provide the required control over the non-dimensional frequencies tested. The pulsator consists of a rotating valve, a reduction mechanism, and a driving motor. A PB100 (PN25) chromium-plated brass full bore valve (diameter 25mm) was modified so that it could rotate 360 degrees, and therefore interrupt the flow of water (generating two pulses per revolution). The rotating valve was driven using an ABB motor (model M2VA71B-2) rated at 0.55 Kw of power. This 3 phase motor was controlled using a control unit also manufactured by ABB. Once a rotating frequency was selected it was kept constant within ± 0.1 Hz. The maximum frequency at which the motor could be rotated was 47.5 Hz, which translates to a maximum rotating frequency of 2.8 Hz for the valve due to the presence of the reduction mechanism.

B. Data Acquisition

A high-speed PIV system was used in order to acquire time-resolved velocity data. This system is comprised of a laser head, a power supply unit, a chiller (used to cool the laser head), a high-speed camera and a PC. Both the laser head and the power supply unit are manufactured by Lightwave Electronics. The laser head consists of a Nd:YAG laser which produces pulses of a wavelength of 532 nm at a maximum power of 100 mW. The system can be triggered internally and externally; if the system is triggered internally it can be operated at frequencies of up to 100 KHz, externally, it can operate up to 16 KHz. In order to maintain the highest possible camera resolution, a maximum operating frequency chosen was 500 Hz. The camera used to capture the images was a HSS-2 HighSpeedStar Video Camera System (LaVision) was used for image capture. This is single frame CCD digital camera with a storage capacity of 1.28 GB (1022 images at highest resolution). It has a spatial resolution of 1280 pixels by 1024 pixels. The TTL trigger for the pulsed experiments was provided by an optical sensor (Monarch Instrument, Model ROS-5W) pointed at the rotating valve. This sensor is needed so that the images for the pulsed experiments can be taken at the

same point in the cycle with an accuracy of 0.005%.

1. Software and Calibration

The image acquistion and post-processing was performed using LaVision Davis 7.0. The calibration plate used was a $80mm$ x 80 mm laminated card, a white background with 225 black crosses. The distance between cross centroid was 5 millimetres. The choice of interrogation window and post-processing was the same for all experiments. A multi-pass (2) decreasing window size algorithm with a 50% overlap was used. The initial interrogation window size was 128x128 pixels and the final window size was 32x32 pixels. Due to the use of window overlapping, the final spatial resolution is 16 pixels.

2. System Accuracy and Error

With the aid of sub-pixel estimators used in Davis, the PIV system is capable of measuring displacements as small as 0.1 pixel. Therefore, the minimum resolved speed is a function of the camera magnification and the acquisition frequency. Based on the highest acquisition frequency and the largest field of view employed, the system accuracy is ± 0.001 m/s. There are many factors that can lead to errors in the calculation of the velocity vectors. These include; the choice of particle, out-of-plane motion, high displacement gradients, laser accuracy, peak-locking, etc. By an appropriate selection of particles (size and density) most of the potential sources of errors can be eliminated or neglected. For the work presented, the diameter of the particles was a concern since it is smaller than 2 pixels, therefore, increasing the chance of peak-locking, so anti-peak-locking algorithms were employed. Vectors were calculated using decreasing window sizes and overlapping, therefore significantly reducing (or eliminating) the bias towards small particle displacements in areas with high velocity gradients. Consequently, it was determined that the main source of error in the velocity calculation originated from the calibration of the camera. In regards to the position of the crosses in the calibrating plate, the least accurate mapping function for the experiments carried out in this investigation gave a standard deviation of 0.2 pixel. Assuming a normal distribution of the crosses, and for a 95% confidence level, a given interrogation window will be located within 0.4 pixel of its measured position. Therefore, for a final interrogation window of 32x32 pixels, the estimated error is $\pm 1.25\%$.

C. Data Analysis

Once the velocity data were extracted from the acquired images using Davis 7.0, any further analysis on the data was perform using Matlab. The velocity statistics for the steady jet were obtained using the well known Reynolds decomposition. However, for the pulsed regime, the velocity statistics were obtained using a triple decomposition of the velocity signal.

1. Reynolds Decomposition

The velocity statistics for steady jets were obtained using the Reynolds decomposition of the velocity signal shown in equation (1), where $u_{(x,r)}$ represents the measured velocity, at axial location x, and radial location r, $U_{(x,r)}$ is the local mean of the velocity signal, and $u'_{(x,r)}$ is the fluctuating part of the velocity component. Furthermore, the turbulent part of the velocity signal can be extracted rearranging equation (1), to obtain equation (2). Using this relation, the turbulent statics can be computed at each position (x, r), over the entire data range, N, using the equations shown in table 1, where N, is the number of vector fields. Finally, the time between vector fields corresponds to $1/f$, where f, is the acquisition frequency.

$$u_{(x,r)} = U_{(x,r)} + u'_{(x,r)} \tag{1}$$

$$u'_{(x,r)} = u_{(x,r)} - U_{(x,r)} \tag{2}$$

2. Triple Decomposition

The velocity signal of the pulsed jets was decomposed using a triple decomposition[10,11] shown in equation (3), where $u_{(x,r)_t}$ is the total velocity or measured velocity, $U_{(x,r)}$ is the time-averaged velocity over all the cycles, $\widetilde{U}_{(x,r)_t}$ is the phase-locked averaged velocity, measured from $U_{(x,r)}$, and finally, $u'_{(x,r)_t}$ is the turbulent

Statistic Type	Equations
Velocity Fluctuations	$u'_{rms(x,r)} = \sqrt{\frac{1}{N}\sum_{i=1}^{N}(u_{i(x,r)} - U_{(x,r)})^2}$
Mean TKE	$k_{(x,r)} = \frac{1}{2N}\sum_{i=1}^{N}(u_{i(x,r)} - U_{(x,r)})^2 + (v_{i(x,r)} - V_{(x,r)})^2$
Reynolds Stresses	$u'v'_{(x,r)} = \frac{1}{N}\sum_{i=1}^{N}(u_{i(x,r)} - U_{(x,r)})(v_{i(x,r)} - V_{(x,r)})$

Table 1. Turbulent quantities equations used for steady jets

or fluctuating component. In addition, x and r, represent the axial and radial locations where the velocity signal is extracted, at time t. In order to reduce computing time, the time-averaged velocity $U_{(x,r)}$, which has a fixed value over time, was combined with the phase-locked average velocity $\widetilde{U}_{(x,r)_t}$ resulting in $\widehat{U}_{(x,r)_t}$, therefore, equation (3), can be rewritten as shown in equation (4), which represents a dual decomposition of the velocity signal. Finally, the turbulent component of the velocity signal can be extracted using equation (5). This process is shown graphically in figure 2. Therefore, $u'_{(x,r)_t}$, represents the turbulent part of the velocity signal at time t of the cycle, but with the cyclic component removed. The relations used in order to calculated the turbulent quantities for pulsed jets are shown in table 2, where N is the total number of velocity fields and t_i represents the time in the cycle that corresponds to a given value of N.

$$u_{(x,r)_t} = U_{(x,r)} + \widetilde{U}_{(x,r)_t} + u'_{(x,r)_t} \tag{3}$$

$$u_{(x,r)_t} = \widehat{U}_{(x,r)_t} + u'_{(x,r)_t} \tag{4}$$

$$u'_{(x,r)_t} = \widehat{U}_{(x,r)_t} - u_{(x,r)_t} \tag{5}$$

Statistic Type	Equations
Velocity Fluctuations	$u'_{rms(x,r)} = \sqrt{\frac{1}{N}\sum_{i=1}^{N}(u_{i(x,r)_{t_i}} - \widehat{U}_{(x,r)_{t_i}})^2}$
Triple Correlations	$u'^3_{(x,r)} = \frac{1}{N}\sum_{i=1}^{N}(u_{i(x,r)_{t_i}} - \widehat{U}_{(x,r)_{t_i}})^3$
Mean TKE	$k_{(x,r)} = \frac{1}{2N}\sum_{i=1}^{N}(u_{i(x,r)_{t_i}} - \widehat{U}_{(x,r)_{t_i}})^2 + (v_{i(x,r)_{t_i}} - \widehat{V}_{(x,r)_{t_i}})^2$
Reynolds Stresses	$u'v'_{(x,r)} = \frac{1}{N}\sum_{i=1}^{N}(u_{i(x,r)_{t_i}} - \widehat{U}_{(x,r)_{t_i}})(v_{i(x,r)_{t_i}} - \widehat{V}_{(x,r)_{t_i}})$

Table 2. Turbulent quantities equations used for pulsed jets

D. Experimental Error and Uncertainty

Table 3 presents a summary of the estimated error for the various turbulent statistics presented in this work. As already mentioned, the accuracy of the velocity measurements is based on the most limiting

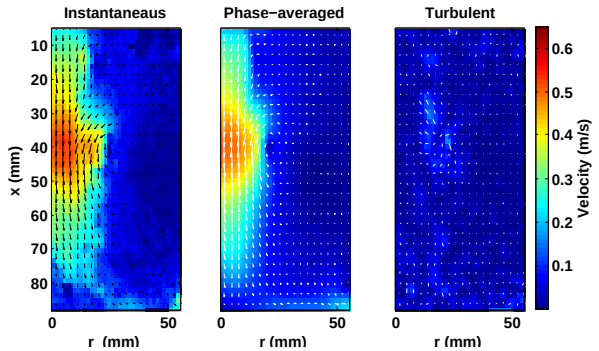

Figure 2. Decomposition of the velocity signal (whole-field)

experiments carried out, giving an accuracy of 0.001 m/s. Also, the estimated error on the instantaneous and time-averaged velocity measurements was estimated at ±1.25%.

Experimental Quantity	Associated Error
instantaneous velocities (u, v)	±1.25%
mean velocities (U, V)	±1.25%
turbulent components (u', v')	±2.00%
velocity fluctuations (u'_{rms}/U_e, v'_{rms}/U_e)	±3.00%
Reynolds stresses ($u'v'/U_e^2$)	±4.50%
TKE (k/U_e^2)	±5.50%

Table 3. Error summary

III. Results and Discussion

The primary aim of the current work is to examine the effect of the non-dimensional frequency, St, on the flow field of turbulent pulsating impinging jets. All the other parameters that affect the flow field of pulsating jets were kept constant ($Re \approx 10200$, $H/d = 3$, and $d = 30.5mm$). The non-dimensional frequency was set at $St = 0$ (steady jet), 0.10 and 0.25 (pulsating jet). A detailed summary of the test conditions is given in table 4

Variables			Temperatures (°C)				Acquisition Information		Exit Conditions			
Re	H/d	St	T_r	T_1	T_2	T_{avg}	Freq. (Hz)	No. Imgs.	U_{min}	U_{max}	U_e	A_N
10000	3	-	19.00	20.50	20.60	20.55	500	3066	-	-	0.330	-
10560	3	0.10	18.00	19.90	20.50	19.75	250	16380	0.121	0.497	0.350	35%
10240	3	0.25	17.90	18.60	19.30	18.95	500	13284	0.223	0.502	0.345	30%

Table 4. Test conditions summary (velocities in m/s)

A. Flow Characterisation

A round nozzle was used in order to provide an axisymmetric jet flow, with the flow demonstrating a good axisymmetry apart from at low Reynolds numbers ($Re < 5,000$), where a slight break in symmetry near the impinging wall for $0.6 < r/d < 1.4$, with a maximum deviation of approximately 18%. This break in symmetry is attributed to laser light reflections present in the near wall region on the left-hand side of the field-of-view which impaired the calculation of the velocity vectors.

The experimental rig was designed to generate impinging jets with a fully developed exit velocity profile. For the steady flow regime, the velocity profiles at exit were fully developed for Reynolds numbers greater than 3,250. However, for the pulsed flow regime, the exit velocity profiles were only fully developed for Reynolds numbers greater than 3,500.

The axial velocity fluctuations at the jet centreline and at 0.5 diameters away from the nozzle exit are shown in figure 3 for a range of different Reynolds numbers. The results of Aydore[12] and Gardon[13] are also

shown for comparison. The correlation shown in figure 3 closely fits the values of the velocity fluctuations within the free jet region of impinging jets. For Reynolds numbers ranging from 3500 (transitional) to 15000, the velocity fluctuations in the flow can be related to the Reynolds number by:

$$\frac{u'^2}{U_e} = -3.1x10^{-6}Re + 0.075$$

The correlation to include jets with higher Reynolds numbers would not be a simple straight line because as the Reynolds number increases to $Re > 20000$, the value of u'_{rms}/U_e tends to an asymptotic value of 0.01.[14,15]

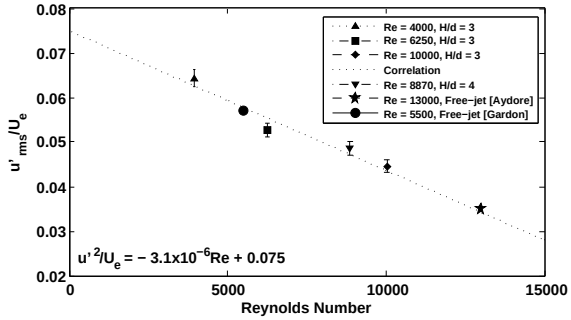

Figure 3. Axial velocity fluctuations in the free jet region ($x/d = 0.5$ and $r/d = 0$)

B. Time-Averaged Flow Field

The effect of the Strouhal number on the time-averaged velocity field of turbulent pulsating impinging jets is shown in figure 4. As the Strouhal number is increased, the jet core spreads more rapidly and the wall jet becomes stronger. This trend is similar to that observed for transitional impinging jets.[16] The pulsating frequency also affects the development of the jet centreline axial velocity, as seen in figure 5, which shows that the centreline velocity decays more rapidly as the Strouhal number is increased. This decay rate is much more rapid than that encountered in a equivalent transitional jet structure[16] (decay commences at $x/d \approx 1.75$ for transitional pulsating jets and at $x/d \approx 1.50$ for turbulent pulsating jets). This indicates that the Reynolds number has a pronounced effect on the centreline velocity decay for pulsating jets, whereas, it has no significant effect on the centreline velocity decay for steady jets. Hence, the effect of the Reynolds number in the presence of a pulsating frequency requires further study.

The development of the mean axial and radial velocity components at various axial locations is shown in figure 6. Near the nozzle exit (figure 6c), the profiles of U/U_e are similar for both of the tested pulsating frequencies and of a similar profile to the steady jet. Further downstream, at $x/d = 2.5$ (figure 6b), although the profiles of U/U_e are almost identical, the profiles of V/U_e show that as the Strouhal number is increased, the jet spreads more rapidly. However, the influence of the Strouhal number is not as strong as that previously observed for the spread of a transitional jet.[16] Close to the impinging wall (figure 6a), the mean axial velocity component is not significantly affected by the pulsating frequency, but it does, however, play an important role in the development of the radial velocity component. As the frequency is increased, the radial velocity component increases - for $St = 0.25$ the radial velocity is approximately 10% larger than that of a steady jet. The frequency also affects the location of the local velocity maximum, with the local maximum shifting away from the stagnation point as St is increased,. Similar to transitional jets, the increase of the radial velocity component near the impinging wall can be attributed to vortex rings impinging on the wall more frequently as the Strouhal number is increased (as shown in figure 7). As the Strouhal number is increased, the vorticity near the surface also increases, indicating that the tangential velocity at the outskirts of the vortex rings is better preserved with increasing St. As a result, when St is increased, not only do the vortex rings reaches the impinging wall more frequently, but it also carries more tangential velocity as it travels across the impinging wall. The movement of the vortex ring away from the centreline, which is caused by the presence of the wall, is then translated into a larger value of the mean radial velocity component near the wall.

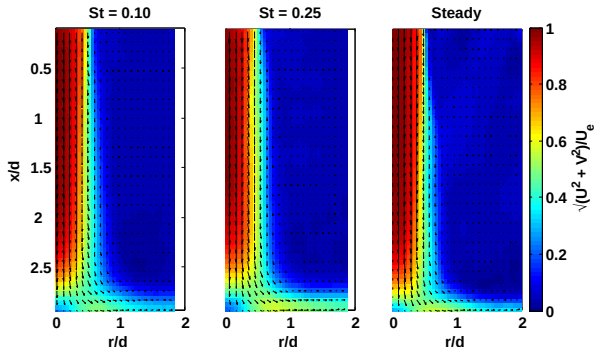

Figure 4. Effect of the Strouhal number on the time-averaged velocity field ($Re \approx 10200$, $H/d = 3$)

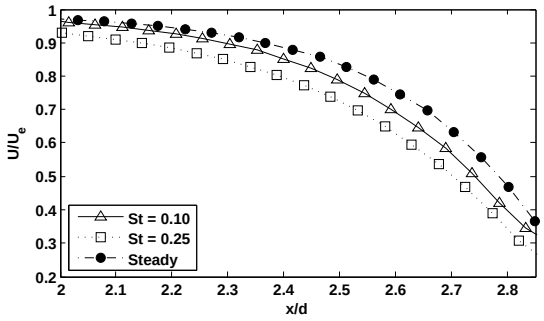

Figure 5. Centreline mean axial velocity decay ($Re \approx 10200$, $H/d = 3$)

C. Velocity Fluctuations

The effect of the Strouhal number in the axial and radial velocity fluctuations on the time-averaged velocity fields are shown in figure 8 and figure 9 respectively. First of all, it can be observed that as the Strouhal number is increased, the axial velocity fluctuations decrease. In contrast, the effect of the pulsating frequency on transitional jets is the opposite.[16] This reduction could be attributed to the fact that the vortex rings are much stronger for turbulent pulsating jets, and therefore less prone to being distorted, and also to the larger exit velocity of the turbulent jet, which leads to a reduction in u'_{rms}/U_e reduce. However, the radial velocity fluctuations increase as the Strouhal number is increased (as shown in figure 9), similar to that observed for comparable transitional jets. This increase in the radial direction could be a result of the increase in the spread of the jet with increasing St since the vortex rings, which carry most of the velocity fluctuations, experience a larger radial displacement. However, this increase is more pronounced for transitional pulsating jets, since the spread of the jet is more dependent on the Strouhal number.

The axial velocity fluctuations at the jet centreline are also affected by St as shown in figure 10. This figure shows that near the nozzle exit, the axial velocity fluctuations increase as the Strouhal number is increased. This increase could be a result of fluid acceleration and deceleration present in this region, which becomes more pronounced as the frequency is increased, leading to higher values of u'_{rms}/U_e. Furthermore, for $x/d > 0.5$ the velocity fluctuations increase steadily, up to approximately $x/d = 2.5$, where the presence of the wall, and velocity deceleration, leads to a decrease in u'_{rms}/U_e. Overall, increasing the Strouhal number leads to an increase of the centreline axial velocity fluctuations.

Figure 11 shows radial profiles of the axial velocity fluctuations at various axial locations. It confirms that throughout the development of the turbulent the jet, for approximately $0.4 < r/d < 0.6$, the effect of the pulsating frequency is to reduce u'_{rms}/U_e, whereas, for transitional jets, increasing the pulsating frequency leads to an overall increase of u'_{rms}/U_e. This indicates that for turbulent impinging jets, the presence of the pulsation helps control the shear layer of the jet and reduces mixing. Nonetheless, outside the shear layer, turbulent pulsating jets, in comparison to steady jets, exhibit similar or slightly larger velocity fluctuations, which are reduced when the Strouhal number is increased.

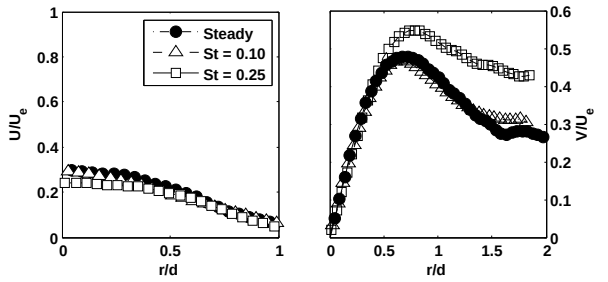

(a) x/d = 2.85

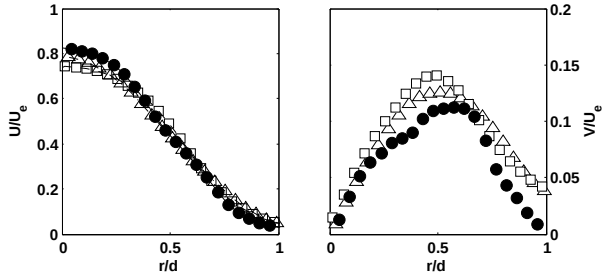

(b) x/d = 2.5

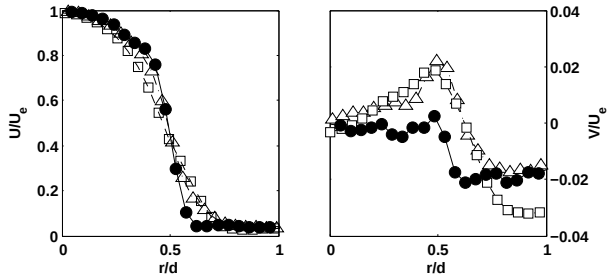

(c) x/d = 0.5

Figure 6. Radial profiles of the mean axial (left) and radial (right) velocity components ($Re \approx 10200$, $H/d = 3$)

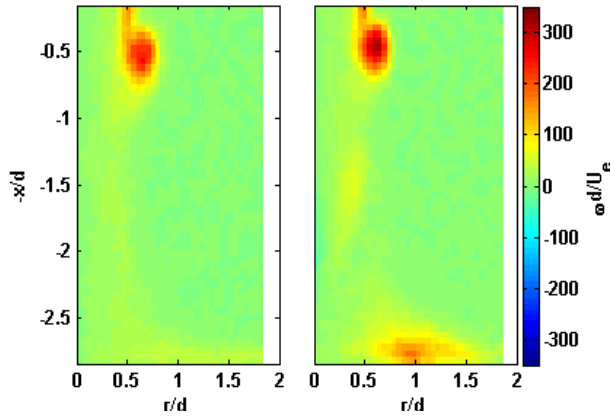

Figure 7. Effect of the Strouhal number on the vorticity field ($Re \approx 10200$, $H/d = 3$)

Finally, figure 9 shows that, within the shear layer, increasing St leads to increases in v'_{rms}/U_e. However, near the impinging wall this effect is reversed (12). The effect of increasing the Strouhal number is similar to the effect observed due to increasing the Reynolds number for steady jets. Therefore, it could be argued that the development of a stronger wall jet as the Strouhal number is increased (see figure 6a) could be the reason for this reduction of v'_{rms}/U_e. However, the radial velocity fluctuations for the pulsed jet are significantly larger than the steady jet, probably as a result of surface renewal caused by the pulses impinging on the wall. An interesting observation is that the behaviour of the velocity fluctuations is significantly more predictable for turbulent pulsating jets than for equivalent transitional pulsating jets.

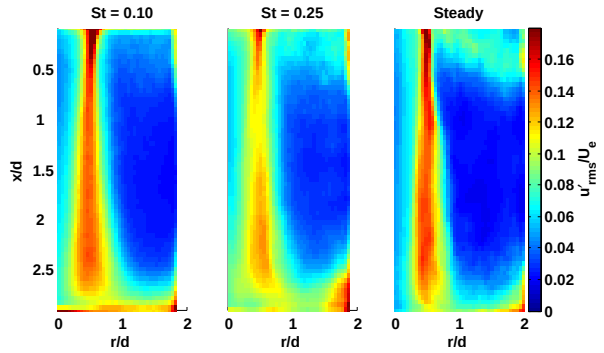

Figure 8. Effect of the Strouhal number on the axial velocity fluctuations ($Re \approx 10200$, $H/d = 3$)

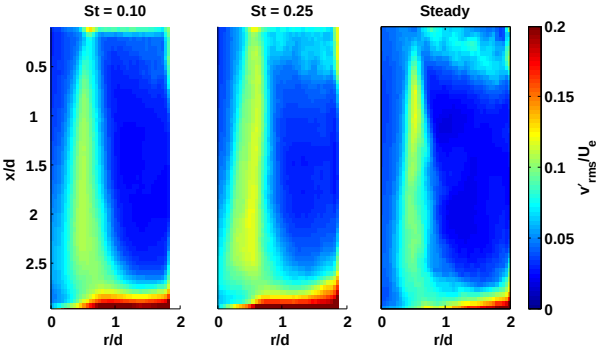

Figure 9. Effect of the Strouhal number on the radial velocity fluctuations ($Re \approx 10200$, $H/d = 3$)

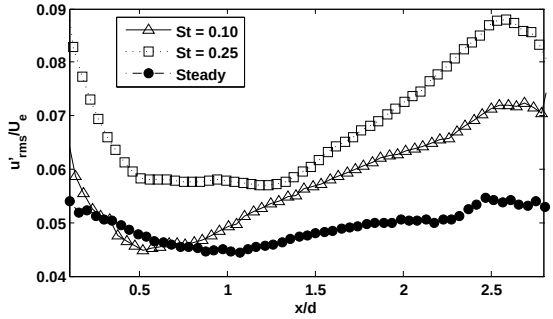

Figure 10. Effect of the Strouhal number on the centreline axial velocity fluctuations ($Re \approx 10200$, $H/d = 3$)

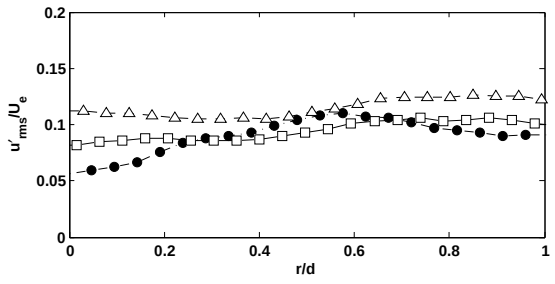

(a) x/d = 2.85

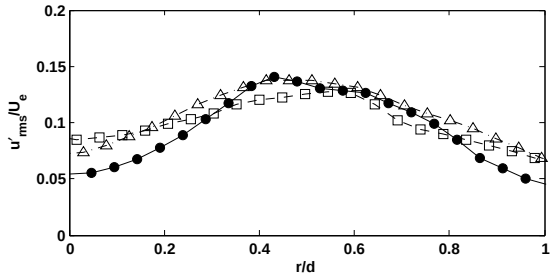

(b) x/d = 2.5

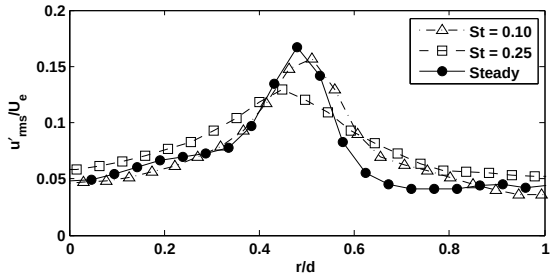

(c) x/d = 0.5

Figure 11. Radial profiles of the axial velocity fluctuations ($Re \approx 10200$, $H/d = 3$)

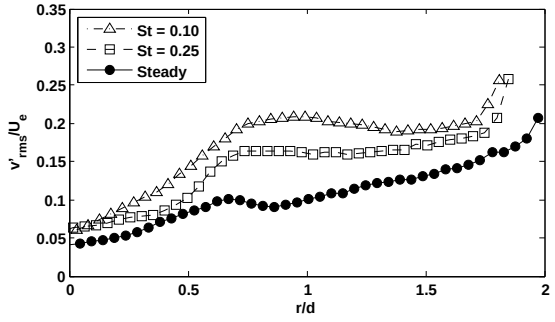

Figure 12. Effect of the Strouhal number on the radial velocity fluctuations near the impinging wall ($Re \approx 10200$, $H/d = 3$, $x/d \approx 2.85$)

D. Turbulent Kinetic Energy

Surface plots of the mean TKE are shown in figure 13. When the Strouhal number is increased from 0 (steady) to 0.10, the mean turbulent kinetic energy within the shear layer of the jet increases. However, as St is further increased to 0.25, there is actually a reduction of the mean turbulent kinetic energy of the jet, in particular, for $0.5 < x/d < 1.5$. This reduction is mainly due to the reduction present in the axial velocity fluctuations (see figure 8 on page 10), which have a significant contribution to the mean TKE. Furthermore, this reduction occurs despite the fact that the radial velocity fluctuations increase with St. This highlights the fact that the axial velocity fluctuations dominate the distribution of the mean TKE within the jet shear layer. Also, this reduction of k/U_e^2 for the jet pulsed at $St = 0.25$ indicates that there is less mixing present within the jet shear layer. Similarly, within the wall jet, the mean turbulent kinetic energy increases as the Strouhal number is increased from $St = 0$ to $St = 0.10$, followed by reduction for $St = 0.25$. This reduction of the mean TKE is linked to the development of a significantly stronger wall jet as the Strouhal number is increased. This trend can be observed in figure 14, which shows that the radial profiles of the mean TKE near the impinging wall exhibit a steady increase from the stagnation point up to $r/d \approx 0.75$, followed by a plateau region ($0.75 < r/d < 1.5$), then a sharp increase for $r/d > 1.5$. These different trends correspond to the acceleration, deceleration, and establishment of the radial velocity near the impinging wall as shown in figure 6a. Finally, the values of k/U_e^2 near the impinging wall are dominated by the radial velocity fluctuations which becomes evident by observing the similarity between the profiles of v'_{rms}/U_e (figure 12 on the previous page) and k/U_e^2 (figure 14).

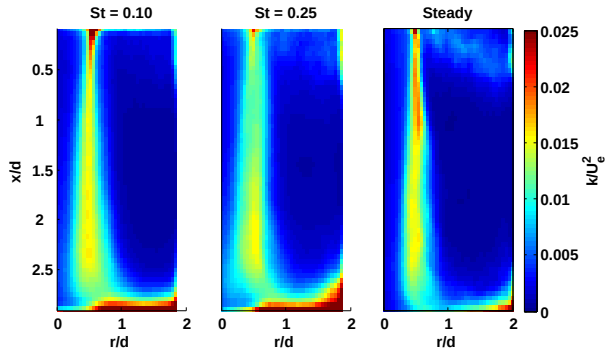

Figure 13. Effect of the Strouhal number on the mean turbulent kinetic energy ($Re \approx 10200$, $H/d = 3$)

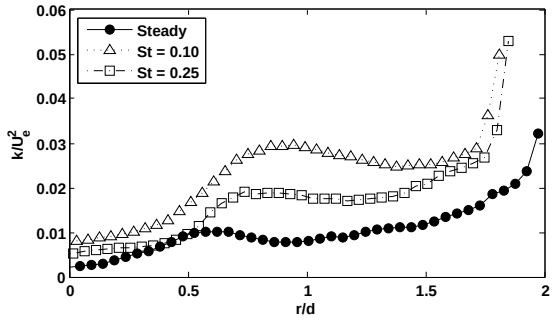

Figure 14. Effect of the Strouhal number on the mean turbulent kinetic energy near the impinging wall ($Re \approx 10200$, $H/d = 3$)

E. Reynolds Stress

Within the wall jet, the Strouhal number affects the distribution of the Reynolds stress. For instance, for the steady jet at $x/d \approx 2.75$ and $r/d \approx 0.75$, ejection (E) Reynolds stress is present, whereas, sweeping (S) Reynolds stress is present for the pulsed jets. Furthermore, farther away from the stagnation point

($x/d \approx 2.75$ and $r/d \approx 1.75$), the steady jet exhibits sweeping (S) Reynolds stress, and the pulsating jets exhibit high-speed fluidic interaction away from the impinging wall (O) instead. Closer to the impinging wall, the pulsating jets exhibit ejection (E) at approximate $r/d = 0.75$, whereas, ejection is present farther away from the wall for steady jets. also, Reynolds stress linked to low-speed fluidic interactions towards the wall (W) are present for all jets. However, as St is increased from $St = 0$ to $St = 0.10$ there is an increase in this type of Reynolds stress, followed by a significant reduction for $St = 0.25$.

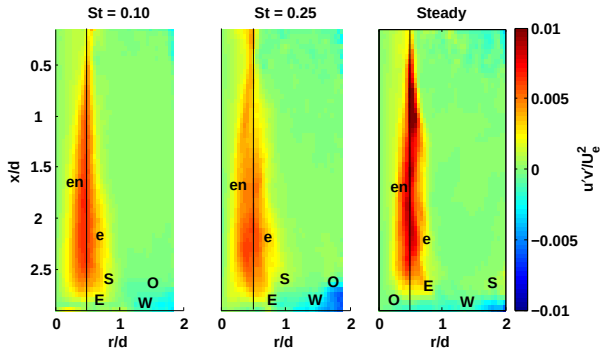

Figure 15. Effect of the Strouhal number on the Reynolds stress; entrainment (en), expulsion (e), ejection (E), sweep (S), wallward interaction (W), outward interaction (O) ($Re \approx 10200$, $H/d = 3$)

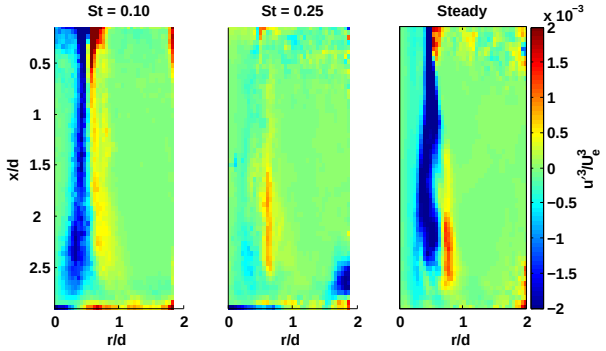

Figure 16. Effect of the Strouhal number on the Skewness Factor $Re \approx 10200$, $H/d = 3$)

The presence of ejection (E) Reynolds stress near the wall for pulsed jets could be due to the impingement of individual pulses on the wall. Finally, the generation of fluidic interactions away from the impinging wall (O) for the pulsating jets could be a result of the pulses carrying momentum away from the surface as they travel along the wall, as suggested by the presence of negative axial skewness factor values in this region (see figure 16). As it can be observed, the momentum transport due to the Reynolds stress is considerably different between steady and pulsed jets, indicating that the heat transfer characteristics would also differ.

IV. Conclusion

A study of the effects of pulsation on a turbulent impinging jet has been peformed. A linear relationship between velocity fluctuations within the turbulent free-jet configuration and the Reynolds number has been observed for the range $Re = 3500 to 15000$ for $H/d > 3$. As the Strouhal number is increased, the jet cone spreads more rapidly, and there is a significant increase in the strength of the wall jet. The effect on the axial and radial components suggests that pulsation acts to control the shear layer and reduce mixing levels, highlighting the dominating influence of the axial velocity fluctuations in the jet shear layer turbulent kinetic energy distribution. Velocity fluctuations in the jet appear to be more readily predicatable than comparative transitional jet cases. Similarities between the turbulent jet structures and comparative steady jet cases suggests that steady jet calculations may be a good baseline for computational studies of pulsating jets.

References

[1]Ma, C. F., Zheng, Q., Lee, S. C., and Gomi, T., "Impingement heat transfer and recovery effect with submerged jets of large Prandtl number liquid - I. Unconfined circular jets," *International journal of heat and mass transfer*, Vol. 40, No. 6, 1997, pp. 1481–1490.

[2]Moreno, O. A., Katyl, R. H., Jones, J. D., and Moschak, P. A., "Mass transfer of an impinging jet confined between parallel plates," *IBM J. RES. Develop.*, Vol. 37, No. 2, March 1993, pp. 143–155.

[3]Nishino, K., Samada, M., Kasuya, K., and Torii, K., "Turbulence statistics in the stagnation region of an axisymmetric impinging jet flow," *International journal of heat and fluid flow*, Vol. 17, 1996, pp. 193–201.

[4]Jamabunathan, K., Lai, E., Moss, M. A., and Button, B. L., "A review of heat transfer data for single circular jet impingement," *International Journal of heat and fluid flow*, Vol. 13, No. 2, June 1992, pp. 106–115.

[5]Sailor, D. J., Rohli, D. J., and Fu, Q., "Effect of variable duty cycle flow pulsations on the heat transfer enhancement for an impinging air jet," *International journal of heat and fluid flow*, Vol. 20, 1999, pp. 574–580.

[6]Mladin, E. C. and Zumbrunnen, D. A., "Local convective heat transfer to submerged pulsating jets," *International journal of heat and mass trasfer*, Vol. 40, No. 14, 1997, pp. 3305–3321.

[7]Zvirin, Y., "Heat transfer between a pulsating impinging jet and a flat surface," *Israel journal of technology*, Vol. 5, No. 1–2, 1967, pp. 152–169.

[8]Poh, H. J., Kumar, K., and Mujumdar, A. S., "Heat transfer from a pulsed laminar impinging jet," *International communications in heat and mass transfer*, Vol. 32, 2005, pp. 1317–1324.

[9]Vejrazka, J., *Experimental study of a pulsating round impinging jet (Etude experimentale d'un jet circulaire impactant pulsant)*, Ph.D. thesis, Laboratoire des ecoulements geophysiques et industriels, Grenoble, December 2002.

[10]Hussain, A. K. M. F. and Zaman, K. B. M. Q., "Vortex pairing in circular jet under controlled excitation. Part 2. Coherent structure dynamics," *Journal of fluid mechanics*, Vol. 101, No. 3, 1980, pp. 493–544.

[11]Bremhorst, K. and Gehrke, P. J., "Measured Reynolds stress distributions and energy budgets of a fully pulsed round air jet," *Experiments in fluids*, Vol. 28, 2000, pp. 519–531.

[12]Aydore, S. and Disimile, P. J., "Natural coherent structure dynamics in near field of fully turbulent axisymmetric jet," *AIAA Journal*, Vol. 35, No. 7, July 1997.

[13]Gardon, R. and Akfirat, J. C., "The role of turbulence in determining the heat transfer characteristics of impinging jets," *International journal of heat and mass transfer*, Vol. 8, 1965, pp. 1261–1272.

[14]Ashforth-Frost, S., Jambunathan, K., Whitney, C. F., and Ball, S. J., "Heat transfer from a flat plate to a turbulent axisymmetric impinging jet," *Proc. instn. mech. engrs.*, Vol. 211, 1997, pp. 167–172.

[15]Baydar, E. and Ozmen, Y., "An experimental and numerical investigation on a confined impinging air jet at high Reynolds numbers," *Applied therman engineering*, Vol. 25, 2005, pp. 409–421.

[16]Medina, H., Benard, E., Huang, J., and Raghunathan, S., "Study of the Fluid Mechanics of Transitional Steady and Pulsed Impinging Jets Using A High-Speed PIV System," 46th AIAA Aerospace Sciences Meeting and Exhibit, AIAA-2008-766, January 2008.